ELSEVIER

www.elsevier.com/locate/ica
Inorganica Chimica Acta 327 (2002) 54–65

Inorganica Chimica Acta

Supported organometallic complexes. Part 27: novel sol–gel processed rhodium(I) complexes: synthesis, characterization, and catalytic reactions in interphases☆

Ekkehard Lindner [a,*], Stefan Brugger [a], Stefan Steinbrecher [b], Erich Plies [b], Michael Seiler [c], Helmut Bertagnolli [c], Peter Wegner [a], Hermann A. Mayer [a]

[a] *Institut für Anorganische Chemie der Universität Tübingen, Auf der Morgenstelle 18, D-72076 Tübingen, Germany*
[b] *Institut für Angewandte Physik der Universität Tübingen, Auf der Morgenstelle 10, D-72076 Tübingen, Germany*
[c] *Institut für Physikalische Chemie der Universität Stuttgart, Pfaffenwaldring 55, D-70569 Stuttgart, Germany*

Received 9 April 2001; accepted 27 July 2001

Dedicated to Professor Kees Vrieze

Abstract

A novel T-silyl functionalized cationic (COD)(dppp)rhodium(I) complex was sol–gel processed with various amounts of the co-condensing agents $MeSi(OMe)_2(CH_2)_6(OMe)_2SiMe$ and $MeSi(OMe)_2(CH_2)_3(C_6H_4)(CH_2)_3(OMe)_2SiMe$ to give novel stationary phases for 'Chemistry in Interphases'. The polysiloxane matrices and the integrity of the rhodium(I) complex centers were investigated by means of multinuclear solid-state NMR (^{13}C, ^{29}Si, ^{31}P) and EXAFS spectroscopies. Dynamic NMR measurements show an increasing mobility of the matrix and the reactive centers with a higher amount of the co-condensing component. The accessibility of the anchored rhodium(I) centers was scrutinized by the metal catalyzed hydrogenation of 1-hexene. All applied xerogels show remarkable activities and selectivities. An enhancement of the activities is achieved when polar solvents are used. SEM micrographs reveal the morphology of the hybrid materials and energy dispersive X-ray spectroscopy (EDX) suggests that the distribution of the elements is in satisfying agreement with the applied composition. © 2002 Published by Elsevier Science B.V.

Keywords: Rhodium(I) complexes; Sol–gel process; Xerogels; Solid-state NMR spectroscopy; EXAFS spectroscopy; EDX measurements; Catalytic reactions in interphases

1. Introduction

In order to achieve the separability of homogenous catalysts from the product, many efforts have been made to heterogenize transition metal complexes [2–6]. Anchoring of reactive centers to polymers [7] or inorganic materials [8,9] entails several momentous disadvantages such as high degree of metal leaching or inhomogeneity of the reactive centers [10]. As an efficient alternative for the reduction or even elimination of these handicaps, 'Chemistry in Interphases' was introduced recently [11]. An interphase is established if a stationary phase and a mobile component penetrate each other on a molecular scale without forming a homogeneous phase. If such interphases are provided with a swellable polymer, they are able to imitate homogenous conditions, because the active centers (e.g. a catalytically active metal complex) become highly mobile simulating the properties of a solution and hence they are accessible for substrates.

Typical interphases are generated by simultaneous co-condensation of T-functionalized ligands or transition-metal complexes with various alkoxysilanes [11,12]. This procedure affords a possibility to modify materials by controlling the density and the distance of the reactive centers [6,13]. Frequently applied co-condensing agents are alkoxysilanes such as $Si(OEt)_4$ ($\mathbf{Q^0}$),

☆ For Part 26 see Ref. [1].

* Corresponding author. Tel.: +49-7071-29 72039/22; fax: +49-7071-29 5306.
E-mail address: ekkehard.lindner@uni-tuebingen.de (E. Lindner).

0020-1693/02/$ - see front matter © 2002 Published by Elsevier Science B.V.
PII: S0020-1693(01)00675-2

$MeSi(OMe)_3$ (**T^0**), and $Me_2Si(OMe)_2$ (**D^0**) [14–18]. By the development of the D-bifunctionalized organosilanes $MeSi(OMe)_2(CH_2)_z(MeO)_2SiMe$ ($z = 6$, 8, 14; **D^0–C_z–D^0**) [19] and $MeSi(OMe)_2(CH)_z(C_6H_4)(CH_2)_z$-$(MeO)_2SiMe$ ($z = 3$, 4; **Ph(1,4-$C_zD^0)_2$**) [20] the highly crosslinked and mobile of Q- and D-groups, respectively have been combined successfully. If these D-bifunctionalized organosilanes are co-condensed with metal complexes or ligands, then highly mobile interphases are formed and the reactive centers are accessible even for large molecules [21–24].

In this work we wish to report on the synthesis and characterization of novel cationic rhodium(I) complexes anchored to polysiloxane-based inorganic–organic hybrid materials. The rhodium centers in these complexes are coordinated to a modified 1,3-bis(diphenylphosphinylpropane) ligand (dppp) [**1(T^0)**] with a spacer of six methylene units. The monomeric T-silyl functionalized complex **2(T^0)** was sol–gel processed with different ratios of the D-bifunctionalized co-condensation agents, **D^0–C_6–D^0** and **Ph(1,4-$C_3D^0)_2$**. Structural investigations of these novel stationary phases were carried out by multinuclear solid-state NMR spectroscopy. With these methods, information on the dynamic properties of the new materials is available [25–27]. An exemplary examination of the coordination sphere of the rhodium(I) center was performed by means of extended X-ray absorption fine structure (EXAFS) spectroscopy, as this method operates in the case of amorphous materials like interphases [19,21]. The morphology of the materials was investigated by scanning electron microscopy (SEM) and the elemental distribution is revealed by EDX spectroscopy. Finally, the accessibility of these polysiloxane-bound complexes was investigated by the catalyzed hydrogenation of 1-hexene.

2. Experimental

2.1. Materials and instrumentation

Elemental analysis was carried out on a Vario EL Analyzer (Elementar Analytische Systeme Hanau). IR data were obtained on a Bruker IFS 48 FT-IR spectrometer. Solution nuclear magnetic resonance spectra were recorded on a Bruker DRX 250 spectrometer (field strength 5.87 T) at 296 K. Frequencies are as follows: ^1H NMR: 250.13 MHz; $^{31}P\{^1H\}$ NMR: 101.25 MHz (referenced to 85% H_3PO_4); $^{13}C\{^1H\}$ NMR: 62.90 MHz. ^{103}Rh NMR resonances were measured using a 2D (^{31}P, ^{103}Rh)$\{^1H\}$ experiment [28]. Chemical shifts in ^1H and $^{13}C\{^1H\}$ NMR spectra were measured relative to the partially deuterated solvent peaks which are reported relative to TMS. The ^{103}Rh chemical shift values are referred to $\Xi(Rh) = 3.16$ MHz [29]. Mass spectra (FD) were acquired on a Finnigan MAT 711A instrument (8 kV, 333 K) and reported as mass/charge (m/z).

CP/MAS solid-state NMR spectra were recorded on Bruker DSX 200 and Bruker ASX 300 (temperature dependent measurements) multinuclear spectrometers equipped with wide bore magnets (field strength 4.7 and 7.05 T). Magic angle spinning was applied at 10 kHz (4 mm ZrO_2 rotors) and 3–4 kHz (7 mm ZrO_2 rotors), respectively. Frequencies and standards: ^{31}P: 81.961 MHz (4.7 T), 121.442 MHz (7.05 T) [85% H_3PO_4, $NH_4H_2PO_4$ (δ 0.8) as second standard]; ^{13}C: 50.228 MHz (4.7 T), 75.432 MHz (7.05 T) [TMS, carbonyl resonance of glycine (δ 176.05) as second standard]; ^{29}Si: 39.73 MHz (4.7 T), 59.595 MHz (7.05 T) (Q_8M_8 as second standard). All samples were packed under exclusion of molecular oxygen. The cross polarization constants T_{XH} were determined by varying the contact time, T_c (14–16 experiments). The proton relaxation times in the rotating frame $T_{1\rho H}$ were measured by direct proton spin lock-τ-CP experiments [30] via ^{29}Si and ^{31}P. The relaxation parameters were obtained using the Bruker software SIMFIT and WINFIT following the procedure described in Ref. [19].

EXAFS measurements were performed at the Rh K-edge (23220 eV) at the beamline X1.1 of the Hamburger Synchrotron–Strahlungslabor (HASYLAB) in DESY, Hamburg with a Si(311) double crystal monochromator under ambient conditions (5.46 GeV, beam current 93 mA). Data were collected in transmission mode with ion chambers. Energy calibration was monitored with a 20 μm thick rhodium metal foil at the K-edge (23 220 eV). All measurements were performed under an inert gas atmosphere. The samples were prepared out of a mixture of the xerogels and polyethylene. Data were analyzed with a program package specially developed for the requirements of amorphous samples [31]. The program AUTOBK of the University of Washington [32] was used for background removal, and the program EXCURV92 [33] was used for the evaluation of the XAFS function. The resulting EXAFS function was weighted with k^3. Data analysis in k space was performed according to the curved-wave multiple-scattering formalism of the program EXCURV92. The mean free path of the scattered electrons was calculated from the imaginary part of the potential (VPI was set to -4.00), the amplitude reduction factor AFAC was fixed at 0.8, and an overall energy shift ΔE_0 was introduced to fit the data. In the fitting procedure the intermolecular coordination numbers were varied and the intramolecular coordination numbers were fixed according to the known values of the ligands around the Rh atom.

The surface areas were determined by analyzing the N_2 adsorption isotherms according to the BET method using a Micromeritics Gemini II.

Scanning electron micrographs and energy dispersive X-ray analysis (EDX) were performed on a Philips XL 30 scanning electron microscope (SEM) equipped with a DX-4 X-ray detection system by EDAX. This consists of an energy dispersive Si(Li)-detector with an active area of 10 mm^2 and the EDX software package. The primary beam energy was set to 20 keV for all measurements. Micrographs were recorded detecting secondary electrons generated by a probe current of 168 pA, whereas 623 pA probe current were applied for carrying out elemental analysis by EDX. Quantification of X-ray emission spectra was achieved employing the ZAF correction procedure to convert X-ray intensities to elemental contents [34]. The sample powder was placed in a specimen stub covered with a conductive adhesive tab and subsequently provided with a sputtered 20 nm gold layer to avoid specimen charging. Owing to its high fluorescence yield, gold emission lines are observed with all spectra. However, the gold layer is too thin to absorb X-rays efficiently and thus does not affect quantification. Spectra were recorded with spot illumination of the sample for 240 live seconds, yielding count rates of about 2000 s^{-1}. Spectra were acquired several times at different sample positions to ensure reproducibility. The various measurements were found to differ by about 3%, which is within the limits of error, especially for light element samples with pronounced topography. Therefore, special care was taken to find specimen areas exhibiting flat surfaces to ensure the validity of the correction models. All measurements were performed at ambient temperature.

All reactions and manipulations were carried out under argon with the usual Schlenk techniques. Methanol was dried with magnesium and distilled. All other solvents were distilled from sodium benzophenone ketyl or calcium hydride. H_2O and $(n\text{-}Bu)_2Sn(OAc)_2$ were distilled under inert gas prior to use. All solvents and reagents were stored under argon. $[\mu\text{-ClRh(COD)}]_2$ [35], the T-functionalized diphosphine **1(T^0)** [36] and the co-condensation agents **D^0–C_6–D^0** [19] and **Ph(1,4-C_3D^0)$_2$** [20] were synthesized as described earlier.

2.2. Catalysis

The hydrogenation experiments were carried out in a 100 ml stainless steel autoclave equipped with a mechanical stirring bar. The autoclave was flushed with argon prior to the introduction of the reaction mixture (1–10 μmol catalyst with respect to rhodium, 6–60 mmol of 1-hexene and 25 ml of the solvent). The suspension was set under hydrogen pressure and stirred prior to heating to the desired temperature. The quantitative analyses were performed on a GC 6000 Vega Series 2 (Carlo Erba Instruments) with an FID and a capillary column CP Sil 88 [17 m, carrier gas helium (50 kPa); integrator Hewlett–Packard 3390 A]. Leaching investigations were carried out with a Varian Spectr AA 20 Plus atomic absorption spectrometer (wave length: 343.5 nm; lamp current: 5 mA; fuel: acetylene; support: air).

2.3. Preparation of η^4-1,5-cyclooctadiene[2-diphenylphosphinylmethyl-1-diphenyl-phosphinyl-8-trimethoxysilyloctanerhodium(I)]hexafluoroantimonate(V) [2(T^0)]

To a solution of $AgSbF_6$ (164 mg, 0.48 mmol) in 3 ml of THF a solution of $[\mu\text{-ClRh(COD)}]_2$ (118 mg, 0.24 mmol) in 3 ml of THF was added under exclusion of light. After stirring for 1 h a solution of **1(T^0)** (295 mg, 0.48 mmol) in 3 ml of THF was added. The reaction mixture was stirred for 2 h and the precipitated AgCl was removed by centrifugation. The solvent was then removed under reduced pressure. The residue was dissolved in 3 ml of THF and 10 ml of n-pentane was added to this solution. After stirring for 10 min, filtration (P3) and drying for 1 h 452 mg (88%) of **2(T^0)** was obtained as a microcristalline, orange–yellow solid. FD MS; m/z: 827.1 ($M^+ - SbF_6$). *Anal.* Calc. for $C_{44}H_{58}F_6O_3P_2RhSbSi$ (MW 1062.1): C, 49.69; H, 5.50. Found: C, 49.32; H, 4.87%. ^1H NMR ($CDCl_3$, δ ppm): 7.56–7.19 (m, 20H, H-phenyl), 4.86, 4.24 [br, 4H, H-olefin (COD)], 3.47 (s, 9H, OCH_3), 2.60–1.05 (m, 23H, CH_2, CH), 0.53–0.47 (m. 2H, CH_2–CH_2–Si). $^{13}C\{^1H\}$ NMR ($CDCl_3$, δ ppm): 134.6–126.3 (m, C-phenyl), 102.2, 95.6 [br, C-olefin (COD)], 48.7 (OCH_3), 38.4 (m, CH_2P), 31.0–20.7 (CH_2, CH), 7.2 (CH_2–CH_2–Si). $^{31}P\{^1H\}$ NMR ($CDCl_3$, δ ppm): 15.5 (d, $^1J_{RhP} = 141.4$ Hz). $^{103}Rh\{^1H\}$ NMR ($CDCl_3$, δ ppm): -350. IR (KBr, cm^{-1}): ν(Si–OMe) 1096, $\nu(SbF_6^-)$ 669.

2.4. General procedure of sol–gel processing

To a solution of **2(T^0)** in 10 ml of THF the corresponding amount of the co-condensing agent **D^0–C_6–D^0** or **Ph(1,4-C_3D^0)$_2$**, 500 mg (28 mmol) of H_2O and the catalyst $(n\text{-}Bu)_2Sn(OAc)_2$ (30 mg, 0.087 mmol) was added. The reaction mixture was stirred at room temperature for 24 h until a gel was formed. The solvent was then removed under reduced pressure and the crude product was dried for 2 h. After washing three times with toluene (5 ml), diethyl ether (5 ml) and n-pentane (10 ml) and drying in vacuum overnight the xerogels **Xa**–**i** were obtained as yellow powders.

Xa: initial weight of **2(T^0)** 513 mg (0.48 mmol). Yield: 467 mg. *Anal.* Calc. for $C_{82}H_{98}F_{12}O_3P_4Rh_2Sb_2Si_2$ (idealized stoichiometry): C, 49.52; H, 4.97. Corrected stoichiometry [19]: C, 49.47; H, 5.06. Found: C, 42.87; H, 3.07% [37][1]. ^{31}P CP/MAS NMR (δ ppm): 15.3. ^{13}C

[1] The low carbon value is due to the incomplete combustion of silicon-containing compounds, which may be responsible for the formation of SiC.

CP/MAS NMR (δ ppm): 144.4–121.1 (br, C-phenyl), 103.8, 98.0 [br, C-olefin (COD)], 40.2, 31.1, 28.8, 23.7, 12.0 (br, CH_2, CH). ^{29}Si CP/MAS NMR (δ ppm): -57.7 (T^2), -64.8 (T^3).

Xb: initial weight of **2(T^0)** 500 mg (0.47 mmol) and of **D^0–C_6–D^0** 345 mg (1.18 mmol). Yield: 730 mg. *Anal.* Calc. for $C_{122}H_{188}F_{12}O_{13}P_4Rh_2Sb_2Si_{12}$ (idealized stoichiometry): C, 48.83; H, 6.31. Corrected stoichiometry [19]: C, 47.87; H, 6.61. Found: C, 42.21; H, 5.13% [37]. ^{31}P CP/MAS NMR (δ ppm): 13.9. ^{13}C CP/MAS NMR (δ ppm): 145.4–120.1 (br, C-phenyl), 103.7, 97.9 [br, C-olefin (COD)], 42.7–10.5 (br, CH_2, CH of backbone and spacer), -0.2 (Si–CH_3). ^{29}Si CP/MAS NMR (δ ppm): -9.8 (D^1), -20.8 (D^2), -57.1 (T^2), -65.4 (T^3).

Xc: initial weight of **2(T^0)** 315 mg (0.38 mmol) and of **D^0–C_6–D^0** 559 mg (1.90 mmol). Yield: 705 mg. *Anal.* Calc. for $C_{162}H_{278}F_{12}O_{23}P_4Rh_2Sb_2Si_{22}$ (idealized stoichiometry): C, 48.49; H, 6.98. Corrected stoichiometry [19]: C, 48.54; H, 6.88. Found: C, 45.44; H, 6.70% [37]. ^{31}P CP/MAS NMR (δ ppm): 14.1. ^{13}C CP/MAS NMR (δ ppm): 145.0–120.3 (br, C-phenyl), 104.2, 98.1 [br, C-olefin (COD)], 49.5 (OCH_3), 44.1–7.3 (br, CH_2, CH of backbone and spacer), -0.4 (Si–CH_3). ^{29}Si CP/MAS NMR (δ ppm): -11.5 (D^1), -22.2 (D^2), -59.0 (T^2), -67.9 (T^3).

Xd: initial weight of **2(T^0)** 185 mg (0.17 mmol) and of **D^0–C_6–D^0** 510 mg (1.74 mmol). Yield: 466 mg. *Anal.* Calc. for $C_{242}H_{458}F_{12}O_{43}P_4Rh_2Sb_2Si_{42}$ (idealized stoichiometry): C, 48.15; H, 7.65. Corrected stoichiometry [19]: C, 46.93; H, 7.57. Found: C, 46.04; H, 7.38% [37]. ^{31}P CP/MAS NMR (δ ppm): 14.1. ^{13}C CP/MAS NMR (δ ppm): 140.2–116.1 (br, C-phenyl), 106.8–90.7 [br, C-olefin (COD)], 49.8 (OCH_3), 44.7–7.9 (br, CH_2, CH of backbone and spacer), -0.2 (Si–CH_3). ^{29}Si CP/MAS NMR (δ ppm): -12.4 (D^1), -22.2 (D^2), -59.0 (T^2), -68.0 (T^3).

Xe: initial weight of **2(T^0)** 205 mg (0.19 mmol) and of **D^0–C_6–D^0** 1130 mg (3.86 mmol). Yield: 1080 mg. *Anal.* Calc. for $C_{402}H_{818}F_{12}O_{83}P_4Rh_2Sb_2Si_{82}$ (idealized stoichiometry): C, 47.88; H, 8.18. Corrected stoichiometry [19]: C, 46.08; H, 8.36. Found: C, 46.63; H, 7.56%. ^{31}P CP/MAS NMR (δ ppm): 14.2. ^{13}C CP/MAS NMR (δ ppm): 145.3–120.8 (br, C-phenyl), 110.5–91.4 [br, C-olefin (COD)], 49.8 (OCH_3), 44.4–8.2 (br, CH_2, CH of backbone and spacer), -0.2 (Si–CH_3). ^{29}Si CP/MAS NMR (δ ppm): -11.5 (D^1), -20.6 (D^2), -56.6 (T^2), -64.2 (T^3).

Xf: initial weight of **2(T^0)** 500 mg (0.47 mmol) and of **Ph(1,4-C_3D^0)$_2$** 437 mg (1.18 mmol). Yield: 665 mg. *Anal.* Calc. for $C_{152}H_{208}F_{12}O_{13}P_4Rh_2Sb_2Si_{12}$ (idealized stoichiometry): C, 53.99; H, 6.20. Corrected stoichiometry [19]: C, 53.04; H, 6.05. Found: C, 53.35; H, 9.23%. ^{31}P CP/MAS NMR (δ ppm): 14.3. ^{13}C CP/MAS NMR (δ ppm): 148.6–115.1 (br, C-phenyl), 103.4–98.5 [br, C-olefin (COD)], 47.1–9.5 (br, CH_2, CH of backbone and spacer), -0.2 (Si–CH_3). ^{29}Si CP/MAS NMR (δ ppm): -9.6 (D^1), -20.5 (D^2), -55.5 (T^2), -65.5 (T^3).

Xg: initial weight of **2(T^0)** 315 mg (0.38 mmol) and of **Ph(1,4-C_3D^0)$_2$** 704 mg (1.9 mmol). Yield: 764 mg. *Anal.* Calc. for $C_{222}H_{318}F_{12}O_{23}P_4Rh_2Sb_2Si_{22}$ (idealized stoichiometry): C, 55.85; H, 6.71. Corrected stoichiometry [19]: C, 54.49; H, 6.69. Found: C, 52.40; H, 6.08% [37]. ^{31}P CP/MAS NMR (δ ppm): 14.0. ^{13}C CP/MAS NMR (δ ppm): 144.4–122.6 (br, C-phenyl), 102.5–95.4 [br, C-olefin (COD)], 49.8 (OCH_3), 44.1–7.3 (br, CH_2, CH of backbone and spacer), -0.1 (Si–CH_3). ^{29}Si CP/MAS NMR (δ ppm): -12.5 (D^1), -21.7 (D^2), -54.7 (T^2), -67.0 (T^3).

Xh: initial weight of **2(T^0)** 185 mg (0.17 mmol) and of **Ph(1,4-C_3D^0)$_2$** 644 mg (1.70 mmol). Yield: 496 mg. *Anal.* Calc. for $C_{362}H_{538}F_{12}O_{43}P_4Rh_2Sb_2Si_{42}$ (idealized stoichiometry): C, 57.52; H, 7.17. Corrected stoichiometry [19]: C, 56.89; H, 7.00. Found: C, 57.90; H, 7.02%. ^{31}P CP/MAS NMR (δ ppm): 10.9. ^{13}C CP/MAS NMR (δ ppm): 149.3–115.8 (br, C-phenyl), 108.4–97.3 [br, C-olefin (COD)], 48.4–8.2 (br, CH_2, CH of backbone and spacer), -0.1 (Si–CH_3). ^{29}Si CP/MAS NMR (δ ppm): -12.8 (D^1), -22.5 (D^2), -67.7 (T^3).

Xi: initial weight of **2(T^0)** 205 mg (0.19 mmol) and of **Ph(1,4-C_3D^0)$_2$** 1430 mg (3.86 mmol). Yield: 1420 mg. *Anal.* Calc. for $C_{642}H_{978}F_{12}O_{83}P_4Rh_2Sb_2Si_{82}$ (idealized stoichiometry): C, 58.73; H, 7.51. Corrected stoichiometry [19]: C, 59.09; H, 7.61. Found: C, 58.74; H, 6.07%. ^{31}P CP/MAS NMR (δ ppm): 14.3. ^{13}C CP/MAS NMR (δ ppm): 148.3–117.9 (br, C-phenyl), 108.3–92.4 [br, C-olefin (COD)], 46.5–8.9 (br, CH_2, CH of backbone and spacer), -0.1 (Si–CH_3). ^{29}Si CP/MAS NMR (δ ppm): -11.8 (D^1), -21.1 (D^2), -54.7 (T^2), -65.8 (T^3).

3. Results and discussion

3.1. Synthesis of the monomeric rhodium(I) complex [2(T^0)]

The cationic rhodium(I) complex **2(T^0)** was obtained in good yields as a orange–yellow microcrystalline powder by the reaction of the diphos ligand **1(T^0)** with a 0.5 equiv. of [μ-ClRh(COD)]$_2$ and 1 equiv. of $AgSbF_6$ (Scheme 1). Complex **2(T^0)** was characterized by ^{1}H, ^{13}C{^{1}H}, ^{31}P{^{1}H}, and ^{103}Rh NMR spectroscopies and mass spectrometry.

3.2. Sol–gel processing of 2(T^0)

The xerogel **Xa** was prepared by sol–gel processing of the monomeric T-functionalized rhodium(I) complex **2(T^0)** without any co-condensing agent, whereas in the case of **Xb–i 2(T^0)** was condensed into a matrix with

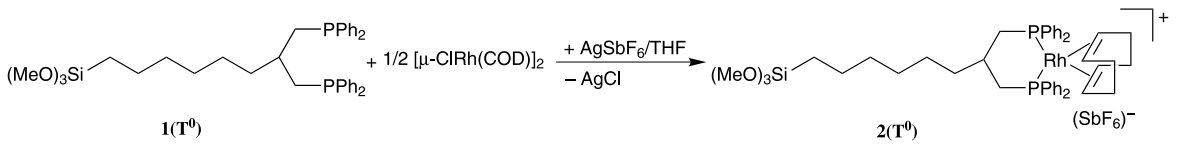

1(T⁰) 2(T⁰)

Scheme 1.

Table 1
Labeling of the compounds

Complex	Co-condensation agent	Ideal T/D ratio	Compound	Xerogel
2(T⁰)			**2a(T″)**	**Xa**
2(T⁰)	**D⁰–C₆–D⁰**	5	**2b(T″)(D^{i}–C₆–D^{i})$_{2.5}$**	**Xb**
2(T⁰)	**D⁰–C₆–D⁰**	10	**2c(T″)(D^{i}–C₆–D^{i})$_{5}$**	**Xc**
2(T⁰)	**D⁰–C₆–D⁰**	20	**2d(T″)(D^{i}–C₆–D^{i})$_{10}$**	**Xd**
2(T⁰)	**D⁰–C₆–D⁰**	40	**2e(T″)(D^{i}–C₆–D^{i})$_{20}$**	**Xe**
2(T⁰)	**Ph(1,4-C₃D⁰)₂**	5	**2f(T″)(Ph(1,4-C₃D^{i})$_2$)$_{2.5}$**	**Xf**
2(T⁰)	**Ph(1,4-C₃D⁰)₂**	10	**2g(T″)(Ph(1,4-C₃D^{i})$_2$)$_{5}$**	**Xg**
2(T⁰)	**Ph(1,4-C₃D⁰)₂**	20	**2h(T″)(Ph(1,4-C₃D^{i})$_2$)$_{10}$**	**Xh**
2(T⁰)	**Ph(1,4-C₃D⁰)₂**	40	**2i(T″)(Ph(1,4-C₃D^{i})$_2$)$_{20}$**	**Xi**

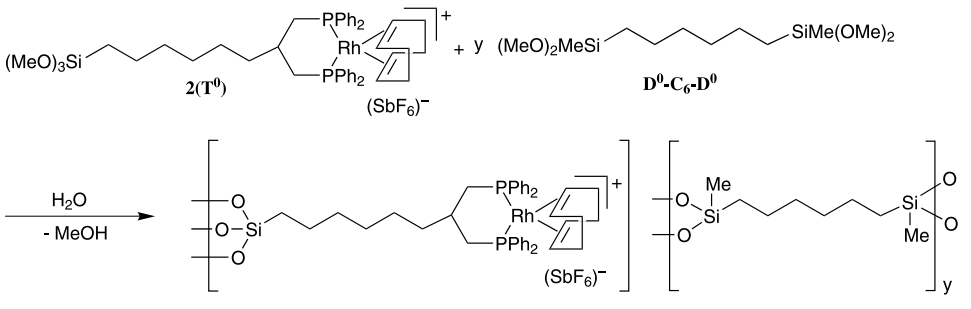

2(T⁰) D⁰-C₆-D⁰

Idealized polycondensation: **2b-e(T^{3})(D^{2}-C₆-D^{2})$_y$**; y = 2.5 (**b**), 5 (**c**), 10 (**d**), 20 (**e**)

Realistic composition: **2b-e(T^{n})(D^{i}-C₆-D^{i})$_y$** (**Xb-e**)

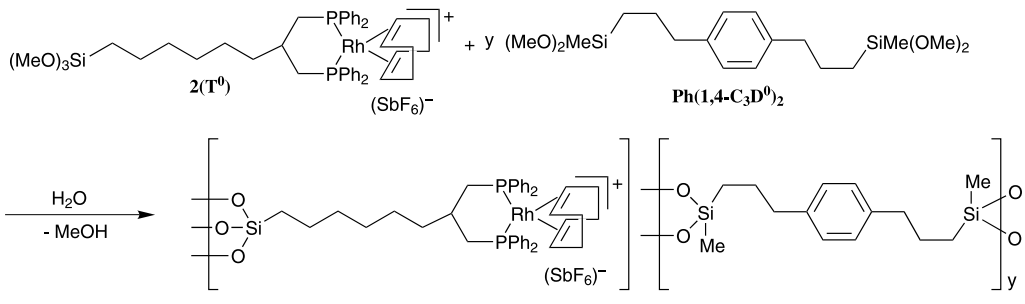

2(T⁰) Ph(1,4-C₃D⁰)₂

Idealized polycondensation: **2f-i(T^{3})[Ph(1,4-C$_3$D^{2})$_2$]$_y$**; y = 2.5 (**f**), 5 (**g**), 10 (**h**), 20 (**i**)

Realistic composition: **2f-i(T^{n})[Ph(1,4-C$_3$D^{i})$_2$]$_y$** (**Xf-i**)

T = T type of silicon atom (three oxygen neighbours)
D = D type of silicon atom (two oxygen neighbours)
i, n = numbers of Si-O-Si bonds (i = 0-2; n = 0-3)

Scheme 2.

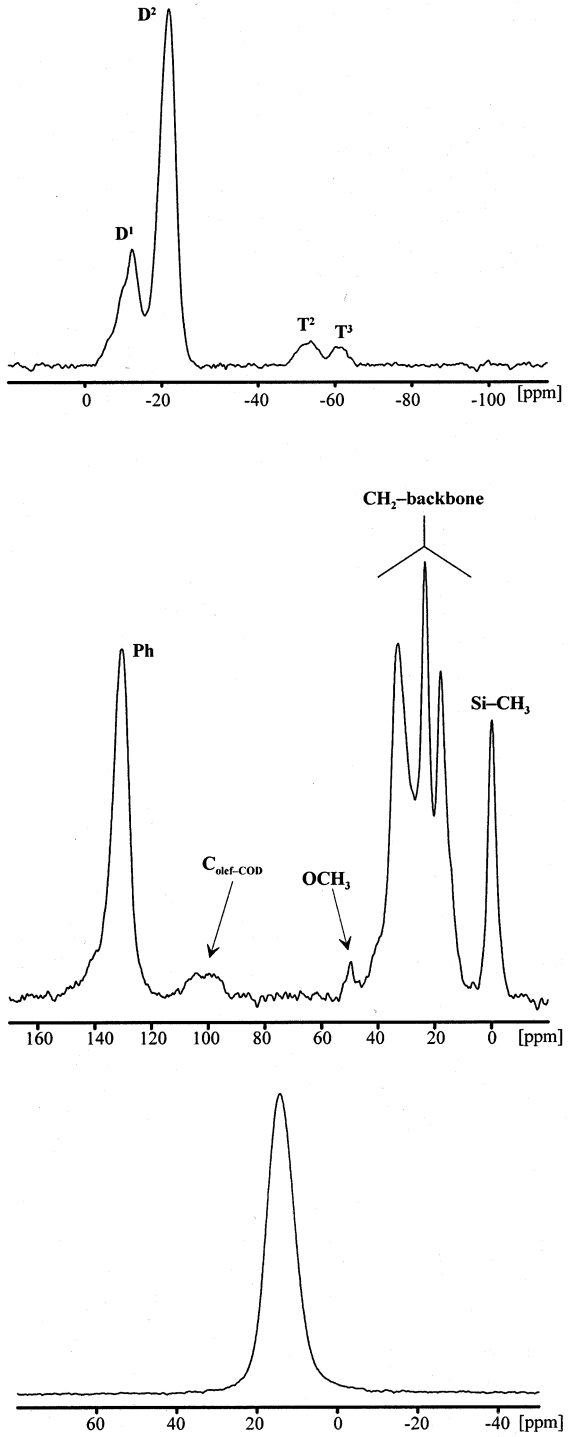

Fig. 1. Solid-state NMR spectra of **Xb**: ^{29}Si CP/MAS (top); ^{13}C CP/MAS (middle); ^{31}P CP/MAS (bottom).

variable amounts of **D^0–C$_6$–D^0** or **Ph(1,4-C$_3$D^0)$_2$** (Table 1, Scheme 2). The properties of such xerogels strongly depend on the reaction conditions during the sol–gel process such as concentration of the monomers, type of solvent, temperature, and kind of catalyst. All sol–gel processes were carried out in THF with an excess of water and (n-Bu)$_2$Sn(OAc)$_2$ as the catalyst. To guarantee reproducible materials uniform reaction conditions were maintained.

3.3. Solid-state NMR spectroscopic investigations

Owing to the amorphous nature of the polymers **Xa**–**i**, solid-state NMR spectroscopy plays an important role in investigating the structure and the dynamic behavior of xerogels [25,26,38]. ^{29}Si NMR spectroscopy enables the characterization of the carrier matrix, the degree of condensation and the stoichiometric composition of the materials. ^{13}C and ^{31}P NMR spectroscopies allow an insight into the hydrocarbon backbone and the reactive center, respectively (Fig. 1).

3.3.1. ^{29}Si CP/MAS NMR spectroscopy

As a result of an incomplete condensation the ^{29}Si CP/MAS NMR spectra of the above-mentioned xerogels reveal signals of various substructures with corresponding D^i- and T^n-functions. Typical chemical shifts are $\delta = -12.5$ (D^1), -21.7 (D^2), -57.1 (T^2), and -67.0 (T^3). They remain unchanged with respect to the stoichiometric ratio between the co-condensation agent and the functionalized rhodium(I) complex. All silicon atoms in the polysiloxane matrix are in direct proximity of protons, thus silyl species are detectable via cross polarization [39,40]. The degree of condensation of D- and T-groups and the real T/D-ratios were determined by contact time variation experiments (Table 2) [19,41]. However, due to the low concentration of the T-functions in the xerogels **Xd**, **e**, **h**, **i** T-groups can hardly be detected. Therefore contact time variation experiments to determine the realistic composition of these xerogels are not feasible within a reasonable time.

With the exception of **Xg** and **Xh**, in the above-mentioned xerogels the degrees of condensation for the D- and T-functions range between 79 and 95%, which is in agreement with the earlier investigations [19,42]. In the case of **Xg** the T-functions show a very low degree of condensation, whereas in the case of **Xh** T- and D-groups are highly condensed. The experimentally determined compositions do not differ significantly from the applied stoichiometries, but it seems that in each sol–gel process a small amount of the D- or T-groups were washed out during the solvent processing.

3.3.2. ^{31}P and ^{13}C CP/MAS NMR spectroscopies

In the ^{31}P CP/MAS NMR spectra of the polysiloxane-bound rhodium(I) complexes **Xa**–**i** only one broad signal is observed with chemical shifts between 10.9 and 15.3 ppm. This result reminds of the monomeric complex measured in solution. No other phosphine species is detectable in the freshly synthesized polymer, but exposure to air for some hours leads to the formation of phosphine oxide resonating at 32 ppm.

The ^{13}C CP/MAS NMR spectra of **Xa**–**e** reveal a broad signal in the aromatic region, which stems from the phenyl carbon atoms of the functionalized dppp ligand. At around 100 ppm, two broad signals occur originating from the olefinic C-atoms of the COD ligand. The resonances of the different methylene carbon atoms between 40 and 10 ppm of **Xa** cannot be resolved. In the case of **Xb**–**e** the aliphatic region is dominated by four major signals resonating at around 33, 23, 18, and 0 ppm, which are assigned to the $\mathbf{D^i}$–$\mathbf{C_6}$–$\mathbf{D^i}$ moiety. In the case of the hybrid polymers **Xf**–**i** all main signals (average shifts: 139.4, 128.9, 39.1, 25.1, 16.8, and −0.3 ppm) with the exception of the peaks originating from the COD ligand at around 100 ppm stem from the $\mathbf{Ph(1,4\text{-}C_3D^i)_2}$ component. The weak or missing signal for the Si–OMe function indicates a very high degree of hydrolysis.

3.4. EXAFS structure determination of the rhodium(I) complexes *Xa*, *Xb*, and *Xf*

The amorphous character of the xerogels makes it impossible to get structural data with conventional X-ray diffraction. However, the properties of EXAFS spectroscopy allow the determination of the local structure around the excited Rh atoms, independent of the samples' physical state. An analysis of the EXAFS provides information on the bond distance, the coordination number, the 'Debye–Waller' factor, and the nature of the scattering atoms surrounding an excited atom [43,44]. The k^3 weighted EXAFS functions (Fig. 2) of **Xa**, **Xb**, and **Xf** can be described by two different atom shells.

For the above-mentioned complexes the first intensive peak in the corresponding Fourier transforms is mainly due to carbon and phosphorus atoms. In the case of **Xa** the assumption of four equivalent carbon atoms with an Rh–C bond length of 2.14 Å leads to a good agreement between the experimental and the calculated functions. Additionally, two equivalent phosphorus atoms were established with an average Rh–P distance of 2.28 Å leading to a significant improvement in the fit (Table 3). In the case of **Xb** the assumption of four equivalent carbon atoms with an Rh–C distance of 2.21 Å and two equivalent phosphorus atoms with an Rh–P bond length of 2.29 Å leads to a good agreement

Table 2
Relative I_0, T_{SiH}, and $T_{1\rho H}$ data of the silyl species in the xerogel

Xerogel	Relative I_0 data of D and T species [a]				Degree of condensation (%)		Real T/D moiety	T_{SiH} (ms) [b]				$T_{1\rho H}$ (ms) [c]
	D^1	D^2	T^2	T^3	D	T		D^1	D^2	T^2	T^3	
Xa			24.0	100		94				0.81	1.34	15.31
Xb	41.1	100	9.8	12.5	85	81	1:6.3	1.44	1.42	1.49	1.60	12.65
Xc	36.3	100	7.3	8.0	87	84	1:8.9	1.34	1.42	1.11	1.25	8.11
Xd	72.4 [d]	100 [d]	2.9 [d]	7.7 [d]	79	91	1:16.4 [d]	1.66	1.97	[e]	[e]	8.02
Xe	31.3 [d]	100 [d]	1.4 [d]	2.5 [d]	88	88	1:33.6 [d]	1.61	1.98	[e]	[e]	2.74
Xf	26.9	100	17.7	19.7	89	82	1:3.4	0.83	0.98	1.04	1.19	11.84
Xg	80.1	100	13.5	8.0	77	73	1:7.9	1.24	1.41	0.92	0.55	5.76
Xh	4.9 [d]	100 [d]	[f]	6.0 [d]	98	100	1:17.4 [d]	[e]	1.00	[f]	1.32	3.31
Xi	10.5 [d]	100 [d]	0.6 [d]	1.5 [d]	95	90	1:52.6 [d]	0.64	0.89	[e]	[e]	1.79

[a] I_0 values calculated according to the literature methods.
[b] Determined by contact time variation.
[c] Determined via ^{29}Si with the experiment according to Ref. [30].
[d] Determined via deconvolution of ^{29}Si CP/MAS NMR spectra ($T_c = 5$ ms).
[e] Intensity to low for a precise determination of T_{SiH}.
[f] Species not detectable.

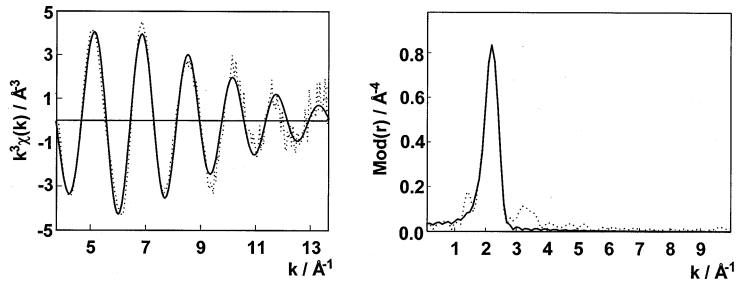

Fig. 2. Calculated (solid line) and experimental (dotted line) $k^3\chi(k)$ function of **Xa** (left) and their Fourier transforms (right) (Rh K-edge) in the k-range 3.85–13.00 $Å^{-1}$.

Table 3
EXAFS-determined structural data of the **Xa**, **Xb**, and **Xf**

	N [a]	**Xa**		**Xb**		**Xf**	
		r (Å) [b]	σ (Å) [c]	r (Å) [b]	σ (Å) [c]	r (Å) [b]	σ (Å) [c]
Rh–C [d]	4	2.14 ± 0.02	0.081 ± 0.01	2.21 ± 0.02	0.059 ± 0.02	2.23 ± 0.02	0.067 ± 0.02
Rh–P [d]	2	2.28 ± 0.02	0.109 ± 0.03	2.29 ± 0.02	0.081 ± 0.01	2.31 ± 0.02	0.063 ± 0.01

[a] Coordination number N.
[b] Interatomic distance r.
[c] Debye–Waller factor σ.
[d] Absorber-backscatterer.

between the experimental and the calculated functions. In the xerogel **Xf** the found Rh–C and Rh–P bond lengths are 2.23 and 2.31 Å, respectively.

The structural data are in a good agreement with the proposed structures of the **Xa**, **Xb**, and **Xf**. Further, in comparison with the structural data of **Xa**, the Rh–C distances of **Xb** and **Xf** are slightly enlarged but still in agreement with the determined bond lengths of similar (COD)diphosphinerhodium(I) complexes [45,46].

3.5. Studies on the dynamic behavior of the xerogels by solid-state NMR spectroscopy

To optimize the stationary component to be employed as catalyst in interphases, it is necessary to get detailed information on the dynamic properties of the materials and reactive centers. Owing to the sensitivity toward motion, NMR parameters like cross-polarization constants and relaxation times give an access to the dynamic properties of materials. Motions in the kilohertz region are responsible for the spin-lattice relaxation time of the protons in the rotating frame ($T_{1\rho H}$), which was determined by a direct spin lock-τ-CP experiment [30] via ^{29}Si and ^{31}P.

3.5.1. Mobility of the matrix

In solid state the xerogels do not differ significantly in the cross polarization constant T_{SiH}. The relaxation time parameter ($T_{1\rho H}$) data extracted from the ^{29}Si CP/MAS NMR measurements of the xerogels depend on the amount of **D^i–C$_6$–D^i** and **Ph(1,4-C$_3$D^i)$_2$** moieties, respectively (Table 2). Shorter $T_{1\rho H}$ values were recorded for a higher amount of the co-condensing agents, thus indicating an increase in the mobility of the matrix, because, according to recent studies the $T_{1\rho H}$ values of the xerogels are considered to reside on the slow motion regime of the correlation time curve [19,23,24]. Comparing the mobilities of the two different co-condensates, it seems that there is no essential difference between the materials with the phenyl ring in the backbone and their counterparts with the alkyl chain as the main building block.

3.5.2. Mobility of the reactive center

Temperature dependent measurements of the $T_{1\rho H}$ values (via ^{31}P) are summarized in Table 4. Owing to the decreasing $T_{1\rho H}$ values in the applied temperature range, all xerogels with the exception of **Xe** and **Xi** reside on the slow motion regime of the correlation time curve [25]. The trend of the $T_{1\rho H}$ values of compounds **Xe** and **Xi** show a similar behavior. First, they decrease, and then they pass through a minimum to increase again with raising temperature. Therefore, these two materials are located in the medium motion regime of the correlation time curve and show the highest mobility of all the xerogels mentioned [25]. These results indicate that the mobility of the reactive centers as well as the mobility of the matrix (vide supra) increases with a higher amount of the co-condensing components. Owing to the electrostatic repulsion of the cationic rhodium(I) centers the space of motion is reduced. If these positively charged complexes are diluted across the carrier matrix, their mobility is enhanced, because of the enlargement of the motion radius.

3.6. Accessibility studies of the anchored rhodium(I) complexes by catalytic reactions

Diphosphinerhodium(I) complexes are applied as catalysts for the hydrogenation of various olefins

Table 4
Temperature dependence of the $T_{1\rho H}$ values

Xerogel	$T_{1\rho H}$ (ms) [a]				
	295 K	305 K	315 K	325 K	335 K
Xa	9.01	[b]	[b]	[b]	[b]
Xb	11.98	10.68	9.94	9.96	[b]
Xc	5.09	7.15	3.81	2.75	[b]
Xd	10.20	11.30	9.36	10.46	8.85
Xe	4.15	1.25	0.91	3.08	3.13
Xf	13.81	13.17	9.22	9.79	8.06
Xg	7.55	10.14	6.21	2.87	[b]
Xh	6.82	5.88	5.30	3.29	2.49
Xi	6.80	0.89	2.62	2.92	[b]

[a] Determination via ^{31}P according to Ref. [30].
[b] Not determined.

Table 5
Hydrogenation of 1-hexene in toluene [a]

Xerogel	Conversion (%)	Hexane (%)	*cis*, *trans* 2-Hexene (%)	TON [b]	TOF [c]
Xa	80.8	61.4	38.6	2811	703
Xb	40.9	86.1	13.9	2136	534
Xc	71.6	77.1	22.9	3326	832
Xd [d]					
Xe	45.7	91.0	9.0	2480	620
Xf	100	84.7	13.3	5035	1259
Xg	40.4	73.3	26.7	1828	457
Xh [d]					
Xi	100	91.9	8.1	5575	1394

[a] Reaction conditions: H_2 pressure 10 bar; Rh:1-hexene = 1:6000; temperature 313 K; reaction time 4 h.
[b] Turnover number ($mol_{sub}\ mol_{cat}^{-1}$).
[c] Turnover frequency ($mol_{sub}\ mol_{cat}^{-1}\ h^{-1}$).
[d] Not determined.

Table 6
Influence of the solvent on conversion and selectivity [a]

Catalyst	Solvent	Conversion (%)	Hexane (%)	*cis*, *trans* 2-Hexene (%)	TON [b]	TOF [c]
Xc	Toluene	71.6	77.1	22.9	3326	832
	1,4-dioxane	75.5	75.5	24.5	3368	842
	methanol	85.5	78.7	21.3	4072	1018
Xg	Toluene	40.4	72.3	26.7	1826	457
	1,4-dioxane	36.7	71.1	28.9	1571	393
	methanol	86.6	76.0	24.0	3968	992

[a] Reaction conditions: H_2 pressure 10 bar; Rh:1-hexene = 1:6000; temperature 313 K; reaction time 4 h.
[b] Turnover number ($mol_{sub}\ mol_{cat}^{-1}$).
[c] Turnover frequency ($mol_{sub}\ mol_{cat}^{-1}\ h^{-1}$).

[45,47–51]. Therefore, the accessibility of the polysiloxane-bound rhodium(I) complexes **Xa**–**c**, **Xe**–**g**, **Xi** was investigated by hydrogenation of 1-hexene (Table 5, Fig. 3). All applied complexes exhibit rather good turnover frequencies in toluene and therefore the metal centers are readily accessible for hydrogen and 1-hexene. However, due to solvation and swelling effects of the anchored rhodium(I) centers and of the matrix, respectively, it seems that there is no predictable correlation between the catalytic activity, selectivity and type of co-condensing moiety.

An enhancement of the conversion rate was achieved with an increase of the solvent polarity (Table 6). In the case of **Xc**, only a slight increase of the activity is observable if dioxane or methanol is used as solvent. The selectivities are comparable in each solvent. In the case of **Xg** the conversion rates and selectivities are comparable in toluene and dioxane, respectively. However, if methanol is used then the selectivity is barely influenced by the solvent but the conversion rate is twice as high compared with the activities in toluene or dioxane. This is another example that the metal catalyzed hydrogenation is favored in polar solvents, especially in alcohols; although these applied inorganic-organic hybrid materials do not exhibit good swelling abilities in polar solvents like methanol [20].

To investigate the stability of the catalysts, the xerogels **Xc** and **Xg** were separated from the reaction mixture and then used again in a catalytic reaction with new solvent and 1-hexene (Table 7). In each case an enhancement of the conversion from run 1 to run 3 was observed, which indicates that the formation of the

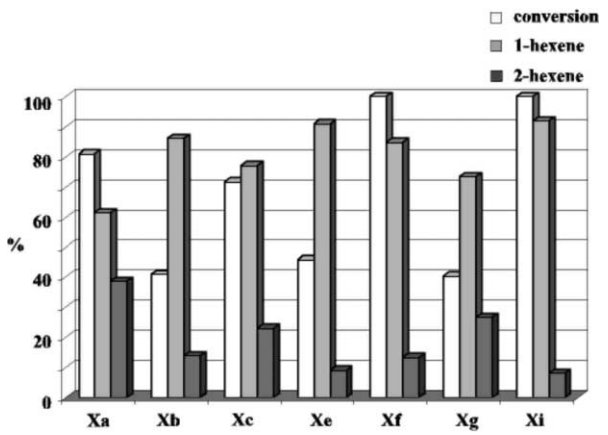

Fig. 3. Catalytic activity of the applied anchored rhodium complexes.

Table 7
Conversions and selectivities of consecutive runs with a recycling of the catalyst [a]

Catalyst	Run no.	Conversion (%)	Hexane (%)	*cis*, *trans* 2-Hexene (%)	TON [b]	TOF[c]
Xc	1	14.2	77.5	22.5	664	332
	2	18.5	65.4	34.6	730	365
	3	31.1	83.0	17.0	1557	778
Xg	1	10.5	67.6	32.4	427	213
	2	27.4	85.4	14.6	1407	703
	3	34.8	67.8	32.2	1419	709

[a] Reaction conditions: toluene as solvent; H_2 pressure 10 bar; Rh:1-hexene = 1:6000; temperature 313 K; reaction time 2 h.
[b] Turnover number ($mol_{sub}\ mol_{cat}^{-1}$).
[c] Turnover frequency ($mol_{sub}\ mol_{cat}^{-1}\ h^{-1}$).

catalytic active species takes place after a relative long period. In the case of **Xc** the selectivity decreases from run 1 to run 2 to increase again in run 3, whereas in the case of **Xg** the highest selectivity was achieved in run 2.

Leaching investigations on the catalysis solution point out, that no rhodium was found to be detached from the polysiloxane support.

3.7. Surface area measurements, SEM images and EDX measurements

Owing to the high organic moieties in these stationary phases, the surface area measurements according to the BET method reveal very low values ($< 3\ m^2\ g^{-1}$), which is in agreement with former results [19,20,52,53].

SEM images of **Xb** and **Xf** are depicted in Fig. 4. Unlike **Xf** the xerogel **Xb** consists of large particles with sharp fracture edges, whereas **Xf** looks cauliflower-like with mainly small-sized particles.

Because of difficulties in classical elemental analysis of Si-containing materials [37] EDX-measurements were carried out. Fig. 5 displays typical EDX spectra of **Xa** and **Xi** including peak assignment. Qualitative analysis confirms the presence of carbon, oxygen, silicon, fluorine, phosphorus, antimony, and rhodium. For quantification purposes, however, the measured composition has to be compared to theoretical values calculated excluding hydrogen, since hydrogen is a single electron atom and thus does not emit characteristic X-rays.

Owing to uncertainties in fundamental parameters at low X-ray energies, spectrometer calibration and the limited detector efficiency in the low energy region, correct quantification of light elements is a principal problem in EDX. Partial line overlap between the P K- and the Au M-line introduces further uncertainties to quantification. Errors are significant for the quantification of minor constituents as the bremsstrahlung background causes signal-to-background ratios below 3 in some cases. However, all elements except for hydrogen can be detected and quantified directly, which is not possible with chemical elemental analysis. In Table 8 the quantification results of the EDX measurements are summarized and compared with the reference data from NMR measurements.

4. Conclusion

Different xerogels **Xa**–**i** were synthesized, in which the T-functionalized (COD)(dppp)rhodium(I) complex [2(**T⁰**)] was incorporated into a polysiloxane matrix.

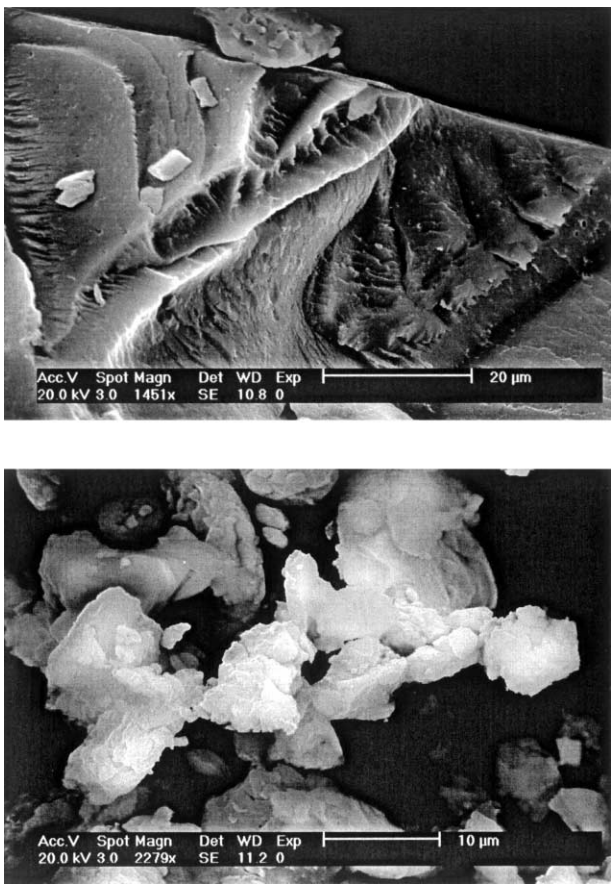

Fig. 4. SEM images of **Xb** (top) and **Xf** (bottom).

Table 8
EDX data of **Xa–i**

Xerogel	Reference data [a]							EDX (ZAF correction) [b]						
	Composition (%) [c]							Composition (%) [c]						
	C	O	Si	P	F	Sb	Rh	C	O	Si	P	F	Sb	Rh
Xa	52.1	2.5	3.0	6.6	12.1	12.8	10.9	55.0	5.7	4.0	6.0	4.6	13.4	11.3
Xb	51.3	9.7	13.2	4.0	7.4	7.8	6.6	55.8	11.5	8.2	4.7	6.4	7.8	5.6
Xc	52.2	9.5	15.8	3.5	6.4	6.8	5.8	51.2	11.1	18.8	3.9	4.7	5.9	4.4
Xd	50.8	14.0	19.3	2.5	4.5	4.8	4.1	49.0	11.6	28.5	2.9	1.8	4.3	1.9
Xe	50.3	17.7	24.5	1.2	2.1	2.3	1.9	52.5	14.5	24.3	1.8	2.3	3.0	1.6
Xf	56.5	6.5	9.5	4.3	7.9	8.3	7.0	55.3	12.6	10.0	3.9	6.0	7.1	5.1
Xg	58.4	9.6	11.8	3.1	5.8	6.1	5.2	61.5	9.5	13.5	3.2	4.2	4.7	3.4
Xh	61.7	9.1	15.5	2.1	3.9	4.2	3.5	61.6	11.3	17.5	1.7	2.9	3.5	1.5
Xi	64.0	11.3	19.5	0.8	1.5	1.6	1.3	62.6	9.4	17.5	1.8	2.7	3.8	2.2

[a] Derived from NMR data according to Ref. [19].
[b] Calculated according to Ref. [34].
[c] Calculated excluding hydrogen.

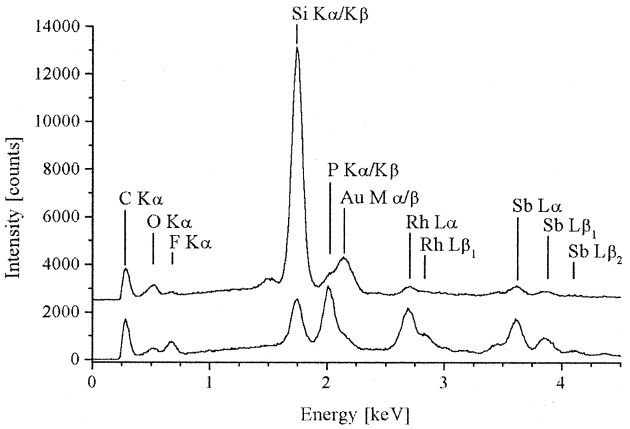

Fig. 5. Typical EDX spectra of **Xa** (bottom) and **Xi** (top). The spectrum of **Xi** is omitted for clarity. Assignment of the characteristic X-ray peaks is indicated. Due to the necessity of a conductive coating, the Au M line is also observed. Partial line overlap of the P K line with the Au M line introduces uncertainties to quantification.

The backbone of the matrices was modified by employment of the different co-condensing agents MeSi-$(OMe)_2(CH_2)_6(OMe)_2SiMe$ (**D^0–C_6–D^0**) and MeSi-$(OMe)_2(CH_2)_3(C_6H_4)(CH_2)_3(OMe)_2SiMe$ [**Ph(1,4-C_3-D^0)$_2$**] in various ratios. Multinuclear CP/MAS NMR spectroscopy and EXAFS studies proved the integrity of the complexes. According to further solid-state NMR experiments, the realistic compositions do not differ significantly from the applied T/D ratios. Studies on the mobility of the matrix and the reactive centers revealed, that an enhancement of the mobility is achieved with a larger amount of the co-condensing components and that both kinds of materials show a similar mobility. The examination of the accessibility of the incorporated rhodium(I) centers within these different types of polysiloxane matrices was carried out by hydrogenation of 1-hexene. All applied materials showed rather good turnover frequencies indicating a good accessibility of the anchored transition metal complexes. Their activity can be increased by using polar solvents. After three runs no reduction of the activity and no metal leaching were observed.

Acknowledgements

The support of this research by the Deutsche Forschungsgemeinschaft (Graduiertenkolleg 'Chemie in Interphasen', Grant No 441/2 Bonn, Bad Godesberg) and by the Fonds der Chemischen Industrie, Frankfurt/Main, is gratefully acknowledged. We thank T. Salesch, Institut für Anorganische Chemie II, University of Tübingen, for BET measurements. We thank Dr. W. Wischert, Institut für Anorganische Chemie II, University of Tübingen, for the AAS measurements. Finally, we thank U. Kehrer, Institut für Anorganische Chemie II, University of Tübingen, for measurement of the ^{103}Rh NMR spectra. We are grateful to Degussa AG, Germany, for a generous gift of $RhCl_3$.

References

[1] E. Lindner, F. Hoehn, T. Salesch, S. Singh, K. Müller, H.A. Mayer, submitted for publication.
[2] P. Panster, S. Wieland, in: B. Cornils, W.A. Herrmann (Eds.), Applied Homogeneous Catalysis with Organometallic Compounds, VCH, Weinheim, 1996.
[3] F.R. Hartley, P.N. Vezey, Adv. Organomet. Chem. 15 (1977) 189.
[4] J. Blum, D. Avnir, H. Schumann, Chemtech 29 (1999) 32.
[5] M. Ann, D.N. Perera, R.J. Angelici, J. Mol. Catal. A 149 (1999) 99.
[6] U. Schubert, N. J. Chem. 18 (1994) 1049.

[7] F.R. Hartley, Supported Metal Complexes, Reidel, Dordrecht, 1985.
[8] D.W. Sindorf, G.E. Maciel, J. Am. Chem. Soc. 105 (1983) 3767.
[9] J. Blümel, Inorg. Chem. 33 (1994) 5050.
[10] I.S. Khatib, R.V. Parish, J. Organomet. Chem. 369 (1989) 9.
[11] E. Lindner, F. Auer, T. Schneller, H.A. Mayer, Angew. Chem. Int. Ed. Engl. 38 (1999) 2154.
[12] E. Lindner, A. Jäger, T. Schneller, H.A. Mayer, Chem. Mater. 9 (1997) 81.
[13] C.J. Brinker, G.W. Scherer, Sol Gel Science, Academic Press, London, 1990.
[14] B. Breitscheidel, J. Zieder, U. Schubert, Chem. Mater. 3 (1991) 559.
[15] R.J.P. Corriu, C. Hoarau, A. Mehdi, C. Reye, Chem. Commun. (2000) 71.
[16] E. Lindner, M. Kemmler, H.A. Mayer, P. Wegner, J. Am. Chem. Soc. 116 (1994) 348.
[17] J. Büchele, H.A. Mayer, Chem. Commun. (1999) 2165.
[18] E. Lindner, R. Schreiber, M. Kemmler, T. Schneller, H.A. Mayer, Chem. Mater. 7 (1995) 951.
[19] E. Lindner, T. Schneller, H.A. Mayer, H. Bertagnolli, T.S. Ertel, W. Hörner, Chem. Mater. 9 (1997) 1524.
[20] E. Lindner, T. Salesch, F. Hoehn, H.A. Mayer, Z. Anorg. Allg. Chem. 625 (1999) 2133.
[21] E. Lindner, A. Baumann, P. Wegner, H.A. Mayer, U. Reinöhl, A. Weber, T.S. Ertel, H. Bertagnolli, J. Mater. Chem. 10 (2000) 1655.
[22] E. Lindner, T. Schneller, F. Auer, P. Wegner, H.A. Mayer, Chem. Eur. J. 3 (1997) 1833.
[23] E. Lindner, S. Brugger, S. Steinbrecher, E. Plies, H.A. Mayer, Z. Anorg. Allg. Chem. 1627 (2001) 1731.
[24] E. Lindner, T. Salesch, S. Brugger, F. Hoehn, P. Wegner, H.A. Mayer, J. Organomet. Chem., in press.
[25] C.A. Fyfe, Solid State NMR for Chemists, CRC Press, Gulph, ON, 1984.
[26] G. Engelhardt, D. Michel, High-Resolution NMR of Silicates and Zeolithes, Wiley, New York, 1987.
[27] H. Eckert, Prog. Nucl. Magn. Reson. Spectrosc. 24 (1992) 159.
[28] R. Benn, C. Brevard, J. Am. Chem. Soc. 108 (1986) 5622.
[29] B.E. Mann, in: P.S. Pregosin (Ed.), Transition Metal Nuclear Magnetic Resonance, Elsevier, Amsterdam, 1991.
[30] R.S. Aujla, R.K. Harris, K.J. Packer, M. Parameswaran, B.J. Say, A. Bunn, M.E.A. Cudby, Polym. Bull. 8 (1982) 253.
[31] T.S. Ertel, H. Bertagnolli, S. Hückmann, U. Kolb, D. Peter, Appl. Spectrosc. 46 (1992) 690.
[32] M. Newville, P. Livins, Y. Yakobi, J.J. Rehr, E.A. Stern, Phys. Rev. B 47 (1993) 14126.
[33] S.J. Gurman, N. Binsted, I. Ross, J. Phys. C 19 (1986) 1845.
[34] J.I. Goldstein, D.E. Newbury, P. Echlin, D.C. Joy, A.D. Romig, C.E. Lyman, C. Fiori, E. Lifshin, Scanning Electron Microscopy and X-Ray Microanalysis, 2nd ed., Plenum Press, New York, 1992.
[35] G. Giordano, R.H. Crabtree, Inorg. Synth. 28 (1990) 88.
[36] E. Lindner, A. Enderle, A. Baumann, J. Organomet. Chem. 558 (1998) 235.
[37] R. Kalfat, F. Babonneau, N. Gharbi, H. Zarrouk, J. Mater. Chem. 6 (1996) 1673.
[38] K. Schmidt-Rohr, H.W. Spiess, Multidimensional Solid State NMR and Polymers, Academic Press, London, 1994.
[39] D.W. Sindorf, G.E: Maciel, J. Am. Chem. Soc. 105 (1983) 3767.
[40] E. Bayer, K. Albert, J. Reiners, M. Nieder, D. Müller, J. Chromatogr. 33 (1983) 197.
[41] R.K. Harris, Analyst 110 (1985) 649.
[42] E. Lindner, W. Wielandt, A. Baumann, H.A. Mayer, U. Reinöhl, A. Weber, T.S. Ertel, H. Bertagnolli, Chem. Mater. 11 (1999) 1833.
[43] E.A. Stern, Phys. Rev. B 10 (1974) 3027.
[44] F.W. Lytle, D.E. Sayers, E.A. Stern, Phys. Rev. B 11 (1975) 4825.
[45] J. Karas, G. Huttner, K. Heinze, P. Rutsch, L. Zsolnai, Eur. J. Inorg. Chem. 3 (1999) 405.
[46] A. Jacobi, G. Huttner, U. Winterhalter, J. Organomet. Chem. 571 (1998) 231.
[47] Y.-Y. Yan, T.V. RajanBabu, Org. Lett. 26 (2000) 4137.
[48] P.A. MacNeil, N.K. Roberts, B. Bosnich, J. Am. Chem. Soc. 103 (1981) 2273.
[49] G. Descotes, D. Lafont, D. Sinou, J.M. Brown, P.A. Chaloner, D. Parker, N. J. Chem. 3 (1981) 167.
[50] U. Nagel, A. Bublewitz, Chem. Ber. 125 (1992) 1061.
[51] O. Pamies, G. Net, A. Ruiz, C. Claver, Eur. J. Inorg. Chem. 9 (2000) 2011.
[52] E. Lindner, S. Brugger, S. Steinbrecher, E. Plies, H.A. Mayer, J. Mater. Chem. 11 (2001) 1393.
[53] E. Lindner, A. Jäger, F. Auer, W. Wielandt, P. Wegner, J. Mol. Catal. A 129 (1998) 91.